Chemical Engineering Journal 255 (2014) 185–194

Contents lists available at ScienceDirect

Chemical Engineering Journal

journal homepage: www.elsevier.com/locate/cej

Ni–Nb mixed oxides: One-pot synthesis and catalytic activity for oxidative dehydrogenation of ethane

José Santander [a], Eduardo López [a], Alejandra Diez [b], Mariana Dennehy [b], Marisa Pedernera [a], Gabriela Tonetto [a,*]

[a] PLAPIQUI (UNS – CONICET), Camino "La Carrindanga" Km 7, CC 717, CP 8000 Bahía Blanca, Argentina
[b] INQUISUR – Dpto. Química, Universidad Nacional del Sur, CP 8000 Bahía Blanca, Argentina

HIGHLIGHTS

- Ni–Nb mixed oxides were prepared by evaporation method and combustion synthesis (CS).
- Ni–Nb catalysts were tested in the oxidative dehydrogenation of ethane to ethylene.
- CS sample showed a very good performance in terms of activity and stability levels.
- Both catalysts presented constant ethylene yields for 240 h in stream at 400 °C.

GRAPHICAL ABSTRACT

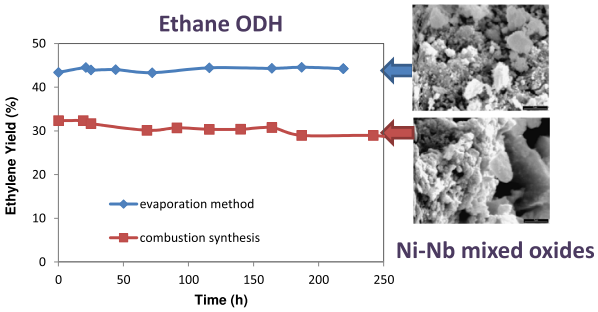

ARTICLE INFO

Article history:
Received 16 February 2014
Received in revised form 28 May 2014
Accepted 11 June 2014
Available online 20 June 2014

Keywords:
Ethylene
Oxidative dehydrogenation
Catalyst synthesis
Nickel
Niobium
Mixed oxides

ABSTRACT

Ni–Nb mixed oxides were prepared by two methods, conventional evaporation method and combustion synthesis. With the latter technique, the mixed oxide can be quickly prepared from an aqueous solution of metal precursors (oxidizers) and sucrose (fuel). The solids with a 0.15/0.85 Nb/Ni atomic ratio were characterized by different techniques including X-ray diffraction, scanning electron microscopy, XPS and Raman spectroscopy, and N_2 adsorption–desorption measurements.

Ni–Nb mixed oxides were tested in the oxidative dehydrogenation (ODH) of ethane to ethylene. The catalyst prepared by combustion synthesis (a technique that is simpler than evaporation method) showed a good performance in terms of activity and stability levels when compared to the catalyst synthesized by the evaporation method, even for long-term runs. Regarding the effect of the metal precursor, nickel nitrate and ammonium niobate oxalate generated the better catalyst in both synthesis routes. Surface activity for ethane consumption and ethylene formation was higher than that observed for the sample prepared by the evaporation method with the same metal precursors.

Both prepared catalysts presented almost constant ethylene yields for 120 h in stream at 400 °C and W/F = 0.06 g s/cm^3 (8% and 15% for combustion and evaporation synthesis, respectively) with a slight decrease over time on stream (13% and 11%).

1. Introduction

Ethylene is a very important olefin in the petrochemical industry; current world production is around 110 million tons per year [1]. Twenty-one percent of ethylene is produced by steam cracking of ethane, and the rest is mainly produced by thermal cracking of petrochemical feedstocks such as naphtha, propane and gas oil [2].

* Corresponding author. Tel.: +54 291 4861700; fax: +54 291 4861600.
E-mail address: gtonetto@plapiqui.edu.ar (G. Tonetto).

http://dx.doi.org/10.1016/j.cej.2014.06.048
1385-8947/

Production of ethylene from ethane can be carried out by thermal or catalytic dehydrogenation processes. However, the thermal process requires operating at high temperatures, with high energy costs and undesired side reactions. The catalytic conversion of ethane under oxidizing conditions is being studied nowadays as an energy-saving method for producing ethylene. Lower reaction temperatures and absence of thermodynamic equilibrium limitations are some of the advantages offered by the catalytic route for the oxidative dehydrogenation (ODH) of ethane.

Several catalytic systems have been employed for ethylene production [3–5]. Mixed oxides present a good catalytic performance in ODH [6–11]. Karamullaoglu et al. [6] investigated the oxidative dehydrogenation of ethane and isobutane using chromium-vanadium-niobium mixed oxide catalysts with different compositions. At 570 °C and with an O_2/C_2H_6 feed ratio of 0.5, ethylene selectivity of about 20% was obtained at a conversion level of 30% over a $Cr_{0.74}V_{0.19}Nb_{0.07}$ catalyst. López Nieto et al. [7] found that a Mo-V-Nb-Te-O mixed oxide catalyst prepared by hydrothermal synthesis presented selectivities to ethylene higher than 80% and ethane conversions higher than 80% operating at relatively low reaction temperatures (340–400 °C). This catalytic behavior was attributed to the formation of a highly selective crystalline phase $Te_2M_{20}O_{57}$ (M = Mo, V, Nb).

NiO is an active but unselective catalyst in the ODH of ethane. The addition of transition metals to the nickel oxide lattice showed to be an effective approach to increase the selectivity in the ODH of light alkanes. Solsona et al. [8,12] studied Ni–W and Ni–Sn mixed oxides in the ODH of ethane. They proposed that nickel sites seem to be the active centers for ethane activation, while the selectivity to ethylene strongly change depending on the Ni/metal ratio. On the other hand, the presence of acid sites facilitates the decomposition of ethylene to CO_2 during ethane oxidation. Heracleous and Lemonidou [13] examined the effect of Li, Mg, Al, Ga, Ti, Nb and Ta. Ni–Nb–O exhibited the best catalytic performance with a 46% ethene yield at 400 °C, while Ni–Li–O presented the worst results with an 8.4% yield. They postulated that dopants can increase or decrease the unselective electrophilic oxygen radicals of NiO, leading to a lower or enhanced ethane ODH activity, respectively.

Ni–Nb mixed oxide catalysts exhibited high activity and selectivity in the ODH of ethane operating at relatively low reaction temperatures [10–14]. Heracleous et al. [10] reported an optimal Nb/Ni ratio of approximately 0.15/0.85 with an overall ethylene yield of 46% at 400 °C. NiO preferentially promoted a total oxidation of ethane due to the electrophilic oxygen species O^- present on the nickel oxide surface. The authors proposed that the addition of Nb to the structure in the NiO lattice reduces the O^- concentration, limiting the total oxidation reaction and consequently increasing the selectivity to ethylene [10,11,15].

According to Savova et al. [11], the formation of a solid solution from both oxides would be limited to Nb concentrations below 1%. They proposed that at low Nb content (up to 3–7%) a part of Nb was spread on the surface of the NiO phase, where it reduced the amount of accessible O^- species. With a niobium loading in the range of 7–15%, the active sites were not modified, and since the specific surface area of the catalysts continued increasing, the ethane conversion increased. This was explained in terms of a "mutual protective effect" between NiO and Nb_2O_5 that prevents the crystallization and/or the growth of NiO particles. With a Nb content over 15%, the inactive $NiNb_2O_6$ phase was formed.

Considering these results, a lower O^- species concentration on the surface of the NiO active phase is key to increase the selectivity in ethane ODH. Another way proposed to decrease the O^- species concentration was the partial reduction of the surface with an organic acid thermally decomposed during catalyst preparation [11]. Recently, a preparation method based on the slow oxidation of a nickel-rich Nb–Ni gel obtained in citric acid was reported [14]. The resulting material had a higher surface area than that obtained by the traditional evaporation method. The most efficient ODH catalysts obtained were those containing 3–4% Nb.

Ni–Nb–O mixed oxides are usually prepared by the evaporation method from nickel nitrate and ammonium niobium oxalate. A simple method for obtaining oxides is the combustion synthesis or the self-propagating high-temperature synthesis [16]. This method consists in inducing the spontaneous combustion of a reactant mixture, placed in an appropriate gas medium. The mixture must have a high chemical energy to produce combustion. Sometimes the heat released by the combustion is not enough for the entire reaction mixture to react. In those cases the combustion may be induced by preheating reactants or by incorporating additives to the reaction mixture [17]. Reaction times are very short and the desired product can be obtained directly after the combustion.

The aim of this study was to evaluate the possibility of using an alternative technique, such as combustion synthesis, to obtain Ni–Nb mixed oxides, active and selective for the ODH of ethane. This method takes advantage of the chemical energy of the reactants, involves few steps, and the reaction occurs quickly [18]. The use of alternative precursors to obtain the mixed oxides was also evaluated.

2. Experimental

2.1. Catalyst preparation

Ni–Nb–O mixed oxides were prepared by the evaporation method (EM) as described in the literature [10], and by one-pot combustion synthesis (CS). The latter was carried out by preparing an aqueous slurry of the precursors with the addition of sucrose in a ratio of 1 mol of sucrose per mol of mixed oxide. The total solids content of the aqueous slurry was 20 wt.%. Sucrose was added to provide the chemical energy needed for combustion. The slurry was placed on a hot plate at 400 °C under continuous stirring until dry. The resulting solid was then heated to 500 °C over the same hot plate in order to obtain spontaneous combustion, yielding a product in fine particulate form. Finally the solid was calcined in flowing air at 450 °C for 5 h.

All the Ni–Nb oxides were prepared with a Nb/Ni molar ratio of 0.15/0.85. The precursor salts used in the reaction were: nickel(II) nitrate hexahydrate ($N_2NiO_6{\cdot}6H_2O$, 99,999%, Aldrich), nickel(II) acetate tetrahydrate ($C_4H_6NiO_4{\cdot}4H_2O$, 99%, Aldrich), ammonium niobate(V) oxalate hydrate ($C_4H_4NNbO_9{\cdot}xH_2O$, 99,99%, Aldrich), and commercial niobia (HY-340, supplied by CBMM-Brazil).

NiO was prepared by thermal decomposition of nickel acetate at 450 °C in air for 5 h.

2.2. Catalyst characterization

The metal content (Ni and Nb) was determined by inductively coupled plasma (ICP). Catalysts' surface areas were determined by N_2 adsorption at 77 K, using the multipoint BET analysis method, with a Quantachrome NOVA 1200e apparatus.

X-ray diffraction (XRD) patterns were obtained using a Philips PW1710 diffractometer, with a monochromatic Cu-Kα source operating at 45 kV and 30 mA.

Particle sizes of the NiO phase in the prepared catalysts were calculated using the Scherrer equation:

$$L = \frac{K\lambda}{B(2\theta\cos\theta)} \quad (1)$$

where L is the mean size of the ordered (crystalline) domains, K is a dimensionless shape factor (0.9), λ is the X-ray wavelength

(λ = 1.5418), B(2θ) is the line broadening at half the maximum intensity (FWHM), and θ is the Bragg angle. Particle sizes were calculated for the highest intensity peak (200). NiO phase lattice parameters were calculated using the following equation:

$$a = d.(h^2 + k^2 + l^2)^{1/2} \quad (2)$$

where a is the lattice parameter, d is the interplanar spacing of the crystal planes, and h,k,l are the Miller Indices. The equation was applied to the highest intensity peak (200).

Temperature-programmed reduction (TPR) was carried out in a conventional apparatus equipped with a thermal conductivity detector (TCD). The samples were pretreated in flowing air at 300 °C for 30 min, followed by flowing Ar treatment for 30 min at the same temperature. After cooling to 25 °C, the temperature was raised to 600 °C at a rate of 10 °C/min in a 5% H_2/Ar flow (50 cm^3/min).

The morphology of the samples was examined by scanning electron microscopy (SEM) on a Jeol JSM 35CF microscope coupled with energy-dispersive X-ray analysis (EDX).

The XPS measurements were conducted using a multi-technique system (SPECS) equipped with a dual Mg/Al X-ray source and a hemispherical PHOIBOS 150 analyzer operating in the fixed analyzer transmission (FAT) mode. The spectra were obtained with pass energy of 30 eV, and the Mg Kα X-ray source was operated at 100 W. The working pressure in the analyzing chamber was less than 2×10^{-8} mbar.

The Raman spectra were recorded using a LabRam HR-UV800/Jobin-Yvon apparatus equipped with a thermal conductivity detector (cooled at 153 K with liquid N_2) and an excitation source of 632 nm.

2.3. Catalytic tests

The ODH of ethane was performed in a fixed bed reactor operating at atmospheric pressure, with a reaction temperature varying between 300 °C and 400 °C. To mitigate thermal effects and looking for isothermal operation, the catalyst particles were mixed with an equal amount of glass particles of small size (40 μm). The feedstock consisted of a mixture of O_2/C_2H_6/He with a 5/5/90 M ratio. The catalyst weight-to-flowrate (W/F) used were equal to 0.06 and 0.54 g s/cm^3 for flowrates of 40 and 20 cm^3/min, respectively. The reaction products were analyzed with an HP Agilent 4890D gas chromatograph equipped with a TCD. Two columns were used in the analysis, a Porapak QS and a Molecular Sieve 5 Å.

3. Results and discussion

3.1. Catalyst characterization

The catalysts were prepared with a molar ratio of Nb/Ni = 0.15/0.85. This selected mixed oxide composition was reported to be the optimum one towards the ODH of ethane, exhibiting the highest levels of activity and selectivity to ethylene [10,11].

The different catalysts prepared in the present contribution synthesized by the two methods already described and from various precursor salts were named as depicted in Table 1.

The compositions, specific surface areas and structure characteristics of the synthesized samples are shown in Table 2. The synthesized solids presented amounts of Nb and Ni very close to the desired optimal composition. The highest value of specific surface area was obtained for catalyst NiNb-E1, approximately 81 m^2/g, in agreement with values reported in the literature [10,11]. Comparing catalysts NiNb-E1 and NiNb-C1, which were prepared with the same precursor salts, it can be observed that the sample prepared by CS presented a lower surface area (25 m^2/g) than that prepared by EM (81 m^2/g). This could be associated with the temperature level reached during CS (1200–3200 °C, depending on the reaction), which was considerably higher than that at which the synthesized catalysts were exposed by the EM procedure. Since CS is known as a very reliable and rapid method to produce catalysts with low particle size and high specific surface area [16], the operating conditions (i.e., fuel loading) could be optimized in order to increase the surface area.

When the precursor salts are compared, in the case of EM, nickel acetate generated a catalyst (NiNb-E2) with lower surface area than nickel nitrate (56 vs. 81 m^2/g), which is the one generally used. In the case of CS, the difference in surface area is more pronounced. NiNb-C2, prepared using niobia, showed almost half the surface area of NiNb-C1 (13 vs. 25 m^2/g). This could be attributed to the fact that Nb_2O_5 does not dissolve and it forms a suspension with the nickel nitrate solution, and then when the combustion takes place, this solid can act as a growth center. The NiNb-C1 catalyst, synthesized from the ammonium niobate oxalate, which is soluble at the beginning of the synthesis, presented an enhanced area and smaller crystal size when compared to the values shown by the NiNb-C2 sample.

Table 1
Nomenclature and catalyst preparation methods.

Preparation method	Evaporation method (EM)		Combustion synthesis (CS)	
Catalyst	NiNb-E1	NiNb-E2	NiNb-C1	NiNb-C2
Precursors	- nickel nitrate - ammonium niobate oxalate	- nickel acetate - ammonium niobate oxalate	- nickel nitrate - ammonium niobate oxalate	- nickel nitrate - niobia

Table 2
Physicochemical characteristics the synthetized catalysts.

Catalyst	Nb/Ni atomic ratio		S_{BET} (m^2/g)	Pore volume (cm^3/g)	Lattice parameter (Å)	Particle size (nm)
	Chemical analysis*	Surface#				
NiNb-E1	0.13/0.87	0.10/0.90	81	0.182	4.1856	22
NiNb-E2	0.12/0.88	0.13/0.87	56	0.135	4.1860	18
NiNb-C1	0.12/0.88	0.12/0.88	25	0.049	4.1861	33
NiNb-C2	0.10/0.90	0.05/0.95	13	0.024	4.1869	45
NiO	0	0	30	0.056	4.1944	46

* Determined by ICP.
\# Determined by XPS.

As seen in Table 2, the catalysts prepared by EM presented higher pore volumes (0.135–0.182 cm^3/g) than NiO (0.056 cm^3/g) and the solids synthesized by CS (0.024–0.049 cm^3/g).

XRD patterns were obtained for the mixed oxides and NiO, as shown in Fig. 1. For the NiNb-E1, -E2 and C1 mixed oxides, peaks corresponding to NiO and a broad background from 2θ between 20° and 35° showing the presence of an amorphous Nb_2O_5 phase were observed. The NiNb-C2 sample exhibited the presence of crystalline Nb_2O_5 and small amounts of the $NiNb_2O_6$ phase. Very weak signals corresponding to $NiNb_2O_6$ were identified in the NiNb-E2, NiNb-C2 and NiNb-C1 samples.

Particle size and lattice parameters determined by XRD patterns are shown in Table 2. The lattice parameter was 4.1944 Å for NiO, and lower for the mixed oxides. The addition of Nb causes a contraction of the NiO lattice. A similar decrease in the size of the NiO unit cell was discussed in terms of a possible substitution of Ni^{2+} by Nb^{5+} [10]. Particle size of the catalysts prepared by EM (22 and 18 Å) was lower than that presented by NiO (46 Å) and CS solids (33 and 45 Å). Particle size for NiNb-C1 (33 Å) also was lower than that for NiO. On the other hand, NiNb-C2 and NiO showed similar crystal sizes. The behavior of NiNb-E1, -E2 and C1 catalysts is typical of this kind of mixed oxides with similar metal content [10,11]. In fact, the addition of niobium in the nickel oxide lattice inhibits crystallization. In the case of NiNb-C2, the two phases (NiO and Nb_2O_5) can be partially segregated and the crystallization of NiO occurs freely, generating large crystals, as in the pure oxide.

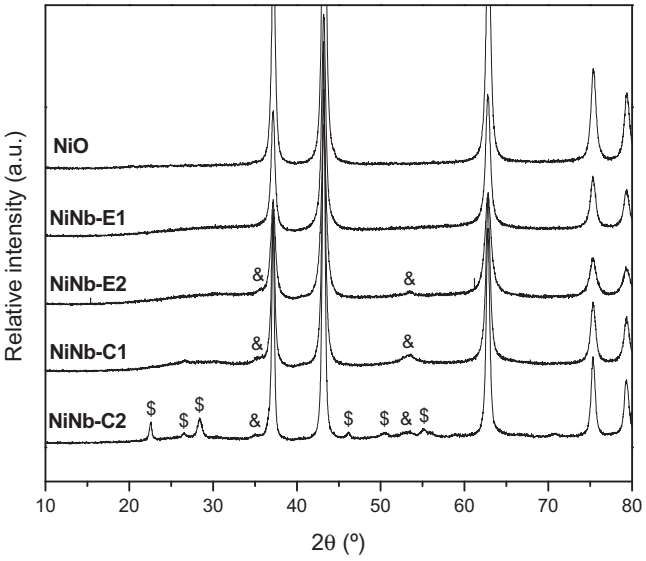

Fig. 1. XRD patterns of the catalysts studied. Ref.: ($) Nb_2O_5 (&) $NiNb_2O_6$.

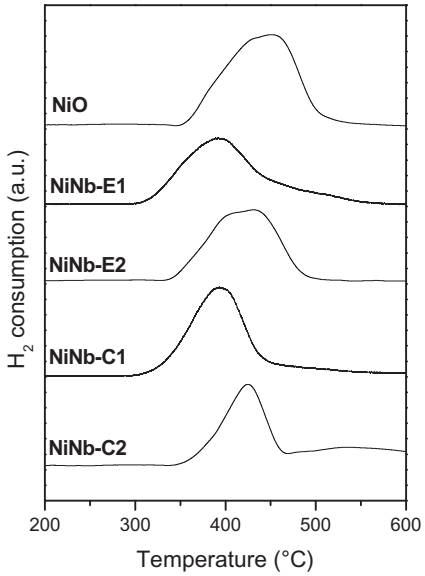

Fig. 2. TPR profiles of the studied catalysts.

TPR patterns of the mixed oxides, and NiO as reference, are shown in Fig. 2. Pure NiO presented a profile with a maximum H_2 consumption at 450 °C. The samples containing Nb showed a shift in the peak towards lower reduction temperatures, in agreement with the literature [10]. NiNb-E1 and NiNb-C1 showed the highest H_2 consumption at 400 °C. In the case of NiNb-E2 and NiNb-C2, the maximum consumption occurred at 430 °C. Nb addition weakened the Ni—O—Ni bonds, as the oxygen can be removed at lower temperatures than in pure NiO [10].

It was verified that Nb_2O_5 is irreducible under the conditions used in the TPR experiment.

Ni–Nb–O samples prepared by CS showed narrow peaks. On the other hand, broad peaks were observed for mixed oxides synthesized by EM. For NiNb-E1, the broad peak extended to about 600 °C. This high temperature shoulder was ascribed to the reduction of Ni–O–Nb hetero-linkages in samples prepared by EM with low Nb content [10]. NiNb-C2 presented a second wide peak at 550 °C that could be assigned to reduction of $NiNb_2O_6$ [19,20], present in this sample. This second peak was not observed for NiNb-C1 or NiNb-E2, where $NiNb_2O_6$ was also detected by XRD.

SEM micrographs of the prepared catalysts are shown in Fig. 3. Both NiNb-E1 and NiNb-E2 samples presented a similar morphology to that of nickel oxide, showing a cluster of small particles. It is important to point out that both oxides and NiO were prepared by EM. The samples synthesized by CS exhibited a more compact structure, due to the probable coalescence of the small particles, specially for NiNb-C2.

The quantitative results of the XPS studies are shown in Table 2. The values of the surface composition were estimated from the Ni 2p and Nb 3d signals, using the appropriate sensitivity correction factors. As shown, the surface Nb/Ni atomic ratios were close to the bulk ratios determined by ICP, except for the NiNb-C2 sample. In this case, the Nb surface composition was lower than the bulk. This could be the consequence of the higher segregation and the existence of the pure oxides that were detected by XRD. The O 1s spectra of the samples, shown in Fig. 4, were used to identify the coexisting oxygen species on the surface of the catalysts. The spectra was deconvoluted into four peaks. These were assigned to O^{2-} lattice oxygen bounded to Ni^{2+} at 529.3–529.8 eV [21] and to Nb^{5+} at 530.0 eV [22,23]. The signal around 531 eV was attributed to oxygen from CO_3^{2-} [24], from an OH^- group bounded to Ni or Nb cations [25], and oxygen atoms adjacent to Ni vacancies (considered as 'defective oxygen') [26]. Higher binding energies (at 531.5–532.5 eV) were ascribed to organic contamination in NiO [26] and O^- species [27]. NiNb-C2 sample showed differences from the rest of the synthesized catalysts. A decrease in the intensity of the peak centered at 530 eV corresponding to O^{2-} lattice bounded to oxygen Nb^{5+} was observed. The decreasing of the signal corresponds to the lower surface concentration of niobium observed for NiNb-C2. XPS spectra of Ni 2p and Nb 3d were measured and analyzed, but no remarkable difference was observed between the catalysts.

Fig. 5 shows the Raman spectra of the Ni–Nb–O catalysts and pure oxides. In the Nb_2O_5 spectrum (thermally pre-treated as the EM mixed oxides), the sharp band near 650 cm^{-1} is related to vibrations of low distorted NbO_6 octahedra [28–31] typical of the TT-Nb_2O_5 phase. The shoulder at 770 cm^{-1} and bands at

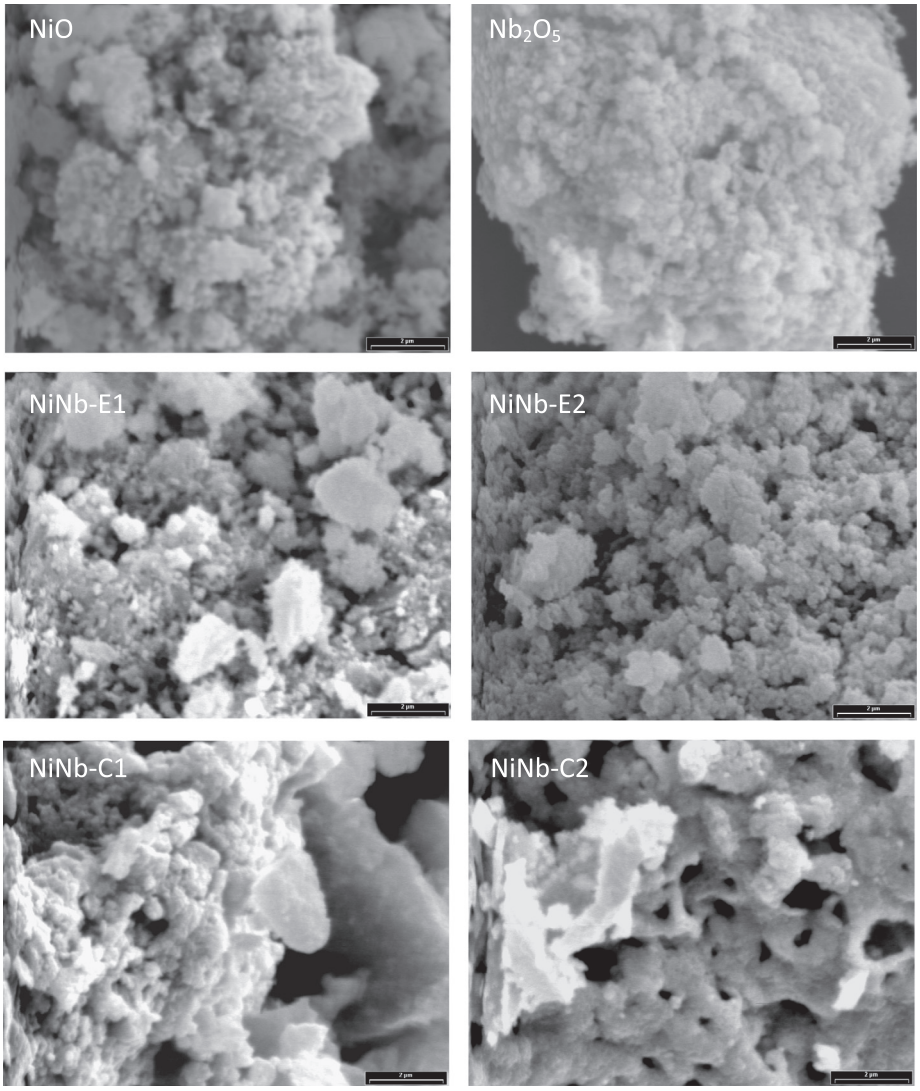

Fig. 3. SEM micrographs of the studied catalysts.

200–300 cm^{-1}s are related to the symmetric and antisymmetric stretching mode of the Nb–O–Nb linkage (high wavenumber region) and the associated bending modes (low wavenumber bands) [28].

The spectrum of pure NiO displays Raman peaks due to a Ni–O stretching mode at 515 cm^{-1} (TO and LO modes) and near 1000 cm^{-1} (2LO modes) [32]. The shoulder at 400 cm^{-1} is related to the non-stoichiometry of the material [33]. In addition, vibrations at 690 and 1060 cm^{-1} were detected, indicating the presence of surface carbonates. Broad bands near 1400 and 1500 cm^{-1} are due to monodentate surface carbonates [34].

For NiNb-C1, the spectrum was very similar to that of Nb_2O_5, typical of Nb_2O_5 TT crystalline phase, with a second shoulder at 900 cm^{-1}. The Raman band at 900 cm^{-1} is due to the small concentration of Nb═O surface sites after the thermal treatment [28]. The band at 500 cm^{-1} is related to the Ni–O stretching mode in NiO.

For NiNb-C1 and NiNb-E1 and E2, the spectra show the band at 500 cm^{-1} associated with NiO, with a lower intensity than in the pure oxide. The addition of Nb to NiO caused the occurrence of the centered band at 840 cm^{-1}. This band is attributed to stretching vibrations of slightly distorted NbO_6 octahedra in amorphous Nb_2O_5 [11]. It is also related to bridging Nb—O—Nb bonds of surface species and/or vibrations of bridging Ni—O—Nb bonds located on the surface of the NiO structure [10].

3.2. Catalytic activity

3.2.1. Catalytic performance in ODH of ethane

The ethane conversion obtained in the catalytic ODH reaction in the 300–400 °C temperature range is presented in Fig. 6. NiNb-C2 showed the lowest paraffin conversion (25% at the highest temperature), followed by NiO. Nb_2O_5 pure oxide (thermally pre-treated as EM catalysts) had no catalytic activity in the studied temperature range. The behavior of NiNb-C2 catalyst can be associated with both the high Nb_2O_5 concentration in the sample and the low surface area. The modification of NiO with Nb generated a crucial change in the catalytic activity. NiNb-E1 catalyst, prepared as reported in [10], showed the highest conversions at the studied temperatures (57.0%), followed by NiNb-C1 with 44.5% at 400 °C. At the same temperature, ethane conversion for NiNb-E2 was 39.4%, slightly lower that for NiNb-C1.

However, experiences not shown in the present manuscript revealed mass transfer limitations when operating at 400 °C for the most active catalysts (NiNb-E1 and NiNb-C1) in the operating

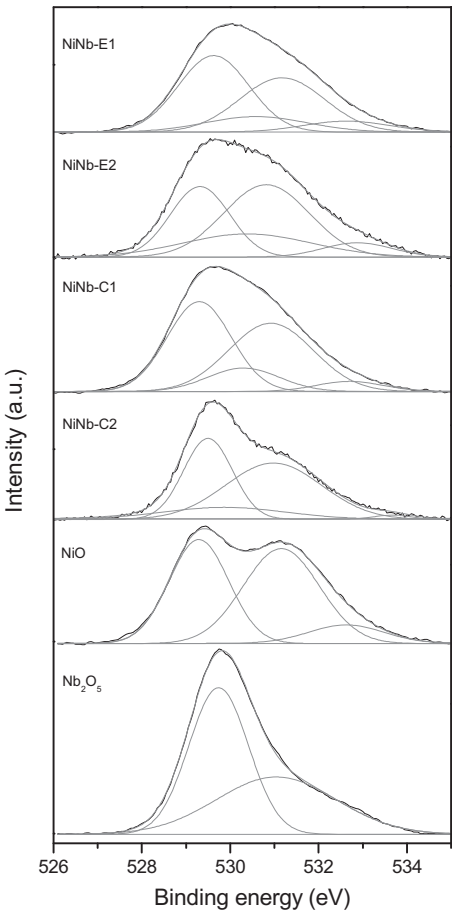

Fig. 4. X-ray photoelectron spectra of the O 1s region of prepared catalysts and reference compounds (niobia and nickel oxide).

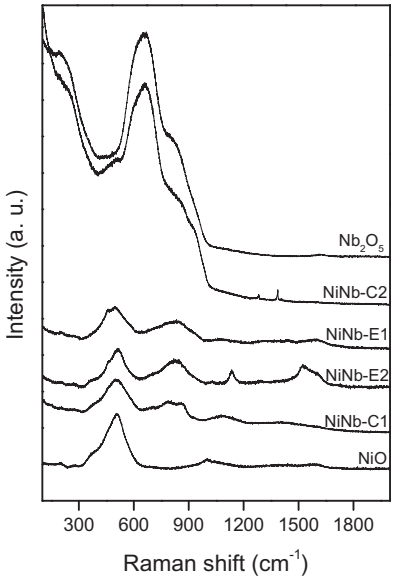

Fig. 5. Raman spectra of the Ni–Nb–O catalysts and pure oxides.

conditions of Fig. 6. Conversely, operation at 350 °C did not present mass transfer limitations at the flowrates selected in all experiences. Fig. 7 presents a catalytic test performed under a high enough flowrate to assure kinetic control ($F = 40\ cm^3/min$ at W/F = 0.06 g s/cm^3). Operation at these conditions led to ethane conversions at 400 °C of 16 and 11% for NiNb-E1 and NiNb-C1, respectively.

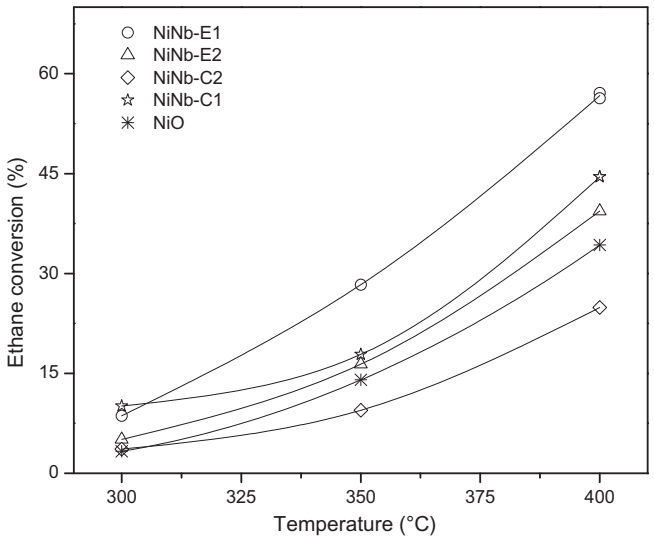

Fig. 6. Ethane conversion as a function of temperature in the ODH reaction (operating conditions: $O_2/C_2H_6/He = 5/5/90$, $F = 20\ cm^3/min$, W/F = 0.54 g s/cm^3).

Table 3 shows ethylene selectivity at 350 °C for the different catalytic samples along with the correspondent conversion attained. NiO and NiNb-C2 presented the lowest selectivities of 19% and 24%. Such low values are typical of Ni oxide; the segregation of Nb_2O_5 in NiNb-C2 led to the similar behavior. NiNb-E2 showed intermediate selectivity of 55%, while the selectivities of NiNb-E1 and NiNb-C1 were 81 and 79% respectively. The difference in selectivity for both evaporation catalysts could be ascribed to the purity of the Ni precursor salt used for each sample, as already referenced in Section 2.1, although no significant differences were measured in Ni/Nb surface ratio (see Table 2). In general, samples showed a slight decrease in selectivity with increasing conversion.

Ethylene yields at 350 °C are reported in Table 3. The value for NiNb-E1 (23.2%) is in agreement with those reported in the literature [10,11]. The change of the Ni precursor salt (nickel acetate for nickel nitrate) in NiNb-E2 resulted in a pronounced drop in ethene yield (9.1%). As expected, NiNb-C2 presented an ethene yield (2.3%) very close to that of pure NiO (2.7%). Catalyst NiNb-C1 showed a yield of 13.8%.

Specific surface activities for both ethylene formation and ethane consumption at 350 °C are also shown in Table 3. It can be observed that NiO exhibited a higher surface reactivity for ethane activation compared with the Ni–Nb mixed oxides prepared by evaporation method (EM), with a poorer ethane selectivity, in agreement with values reported elsewhere [10,11,35]. On the other hand, the performance of NiNb-C1 was remarkable, showing the highest intrinsic rates of ethane consumption (2.7×10^{-8} mol/m^2 s) and ethylene formation (2.1×10^{-8} mol/m^2 s). The combustion synthesis generated a more active catalytic surface when compared to NiO in terms of ethane activation, and more effective in ethylene formation. This catalytic performance could be associated to a better utilization of the active sites due to a higher accessibility of the reagents to the catalyst surface, considering the observed similarities in the chemical aspects of the surface but observed differences in the morphological properties.

3.2.2. Study of catalyst stability

The stability of the prepared mixed oxides was evaluated by means of long-term reaction tests. The catalysts were subjected to reaction for 120 h, without interruption, at 400 °C. Catalytic

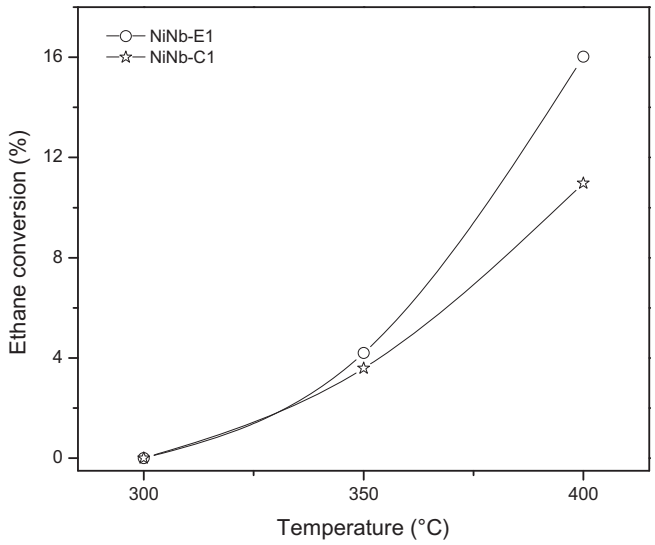

Fig. 7. Ethane conversion as a function of temperature in the ODH reaction (operating conditions: $O_2/C_2H_6/He = 5/5/90$, $F = 40\ cm^3/min$, $W/F = 0.06\ g\ s/cm^3$).

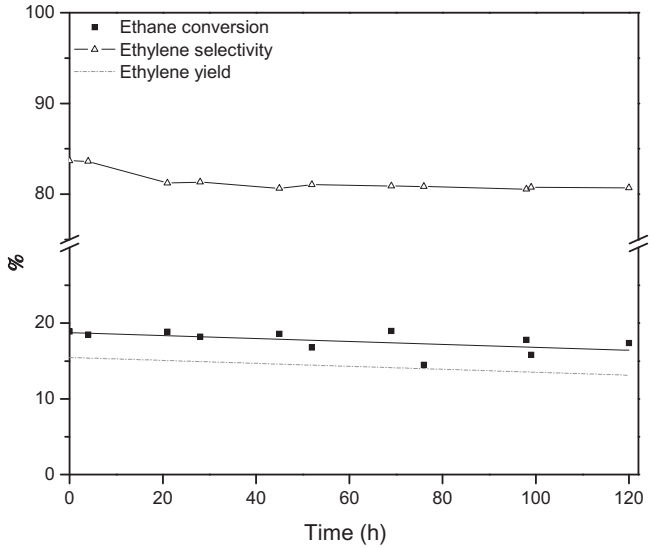

Fig. 8. Ethane conversion and ethylene selectivity and yield as a function of time-on-stream for NiNb-E1 (operating conditions: $O_2/C_2H_6/He = 5/5/90$, $F = 40\ cm^3/min$, $W/F = 0.06\ g\ s/cm^3$, $T = 400\ °C$).

Table 3
Ethane conversion (X), selectivity (S) and yield (Y) in ethylene, and specific surface activity for ethylene formation (r_{C2H4}) and ethane consumption (r_{C2H6}) at 350 °C (operating conditions: $O_2/C_2H_6/He = 5/5/90$, $F = 20\ cm^3/min$, $W/F = 0.54\ g\ s/cm^3$).

Catalyst	X (%)	S (%)	Y (%)	r_{C2H4} (mol/m^2 s)	r_{C2H6} (mol/m^2 s)
NiNb-E1	28.3	81.8	23.1	1.1×10^{-8}	1.3×10^{-8}
NiNb-E2	16.4	55.6	9.1	5.9×10^{-9}	1.1×10^{-8}
NiNb-C1	17.8	77.3	13.8	2.1×10^{-8}	2.7×10^{-8}
NiNb-C2	9.5	24.3	2.3	6.6×10^{-9}	2.7×10^{-8}
NiO	14.0	19.1	2.7	3.0×10^{-9}	1.8×10^{-8}

tests were performed under kinetic control conditions ($F = 40\ cm^3/min$ at $W/F = 0.06\ g\ s/cm^3$). The NiNb-E1 and NiNb-C1 samples were chosen for the stability test due to their better catalytic performance compared to the rest of the catalysts studied. Conversion, selectivity and ethylene yield as a function of time are presented for both catalysts in Figs. 8 and 9, respectively.

In the case of the NiNb-E1 sample (Fig. 8), it was observed that both initial selectivity (84%) and conversion (19%) showed a decrease over time-on-stream (3.5% and 8%, respectively after 120 h). Thus, the ethylene yield after the test presented a drop of 11%. For NiNb-C1 sample, Fig. 9 shows a total decrease of 18% in conversion (with an initial value of 10%) and an increase of 1.3% in selectivity over time-on-stream. Since both variables affect the yield, the sample exhibited a drop after 120 h of reaction (from 8% to 7%).

In order to evaluate the performance of the catalysts in operating conditions leading to a higher ethylene yield, the samples were tested at a lower flowrate of $F = 20\ cm^3/min$ for $W/F = 0.54\ g\ s/cm^3$, although operation under pure kinetic control could not be assured.

In the case of the NiNb-E1 sample (Fig. 10), it was observed that both selectivity (72%) and conversion (61%) remained constant over time-on-stream. Thus, the ethylene yield after the test was similar to the initial value (44%). Focusing the behavior of NiNb-C1 catalyst, Fig. 11 shows a total decrease of 18% in conversion (from 44% to 36%) and an increase of 9% in selectivity (from 73% to 80%) over time. Since both variables affect the yield, the sample exhibited only a slight drop after 240 h of reaction (from 32% to 29%). After reaction, the samples were named NiNb-E1R and NiNb-C1R.

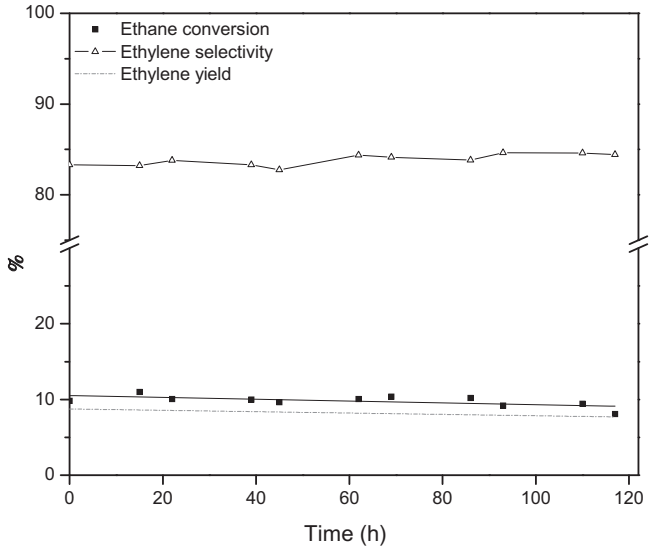

Fig. 9. Ethane conversion and ethylene selectivity and yield as a function of reaction time in the ODH reaction over NiNb-C1 (operating conditions: $O_2/C_2H_6/He = 5/5/90$, $F = 40\ cm^3/min$, $W/F = 0.06\ g\ s/cm^3$, $T = 400\ °C$).

The spent catalysts (after 240 h on stream) were characterized. The stability of the phases present in the studied oxides was determined by analyzing X-ray diffraction patterns before and after the reaction (Fig. 12). For catalyst NiNb-E1, the appearance of the $NiNb_2O_6$ phase was observed after the test. In the case of the sample NiNb-C1, a slight increase in the intensity of the peaks corresponding to the $NiNb_2O_6$ phase was observed during the test. The formation of the $NiNb_2O_6$ phase was reported by Savova et al. [11] for similar catalysts at 380 °C.

Regarding the TPR profiles, it was observed that the samples analyzed after reaction presented a shift towards higher temperatures (of 10 °C for NiNb-E1 and 40 °C for NiNb-C1) compared with the results obtained for the fresh catalysts (see Fig. 13). The shoulder in the NiNb-E1 sample transformed into a second wide peak at 550 °C in NiNb-E1R, which can be ascribed to $NiNb_2O_6$ reduction.

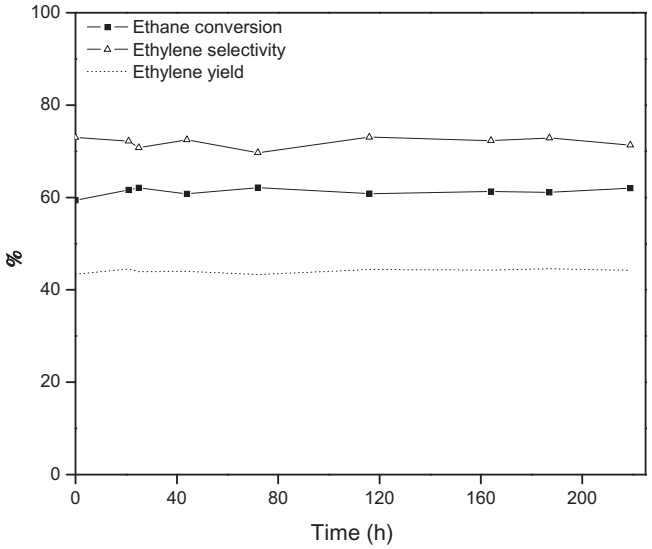

Fig. 10. Ethane conversion and ethylene selectivity and yield as a function of time-on-stream for NiNb-E1 (operating conditions: $O_2/C_2H_6/He = 5/5/90$, $F = 20\ cm^3/min$, $W/F = 0.54\ g\ s/cm^3$, $T = 400\ °C$).

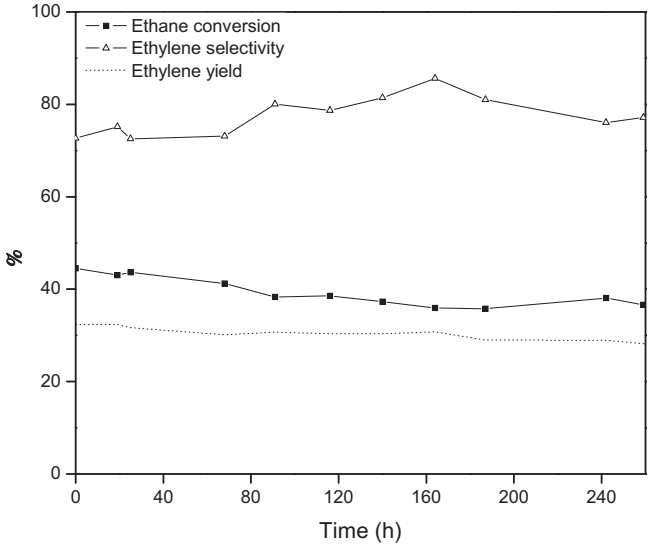

Fig. 11. Ethane conversion and ethylene selectivity and yield as a function of reaction time in the ODH reaction over NiNb-C1 (operating conditions: $O_2/C_2H_6/He = 5/5/90$, $F = 20\ cm^3/min$, $W/F = 0.54\ g\ s/cm^3$, $T = 400\ °C$).

The temperature shift was also related to the formation of this phase.

When analyzing the morphological properties of the solids (Table 4), the decrease in specific surface area (46%) and pore volume (30%) in NiNb-E1R is evident. In the case of NiNb-C1R, the reduction in specific area was lower (20%) and the pore volume remained almost constant.

The quantitative results of the XPS studies indicated that the Nb/Ni surface ratio for the spent catalysts remained constant. As shown in Fig. 14, spectra of fresh and spent catalysts did not show significant changes in the relative intensity of the coexisting oxygen species. XPS spectra of Ni 2p and Nb 3d did not show noticeable differences between spent and fresh catalysts.

Fig. 15 shows Raman spectra of the fresh and spent Ni–Nb–O catalysts. The more notable difference is the appearance of strong bands at 1350 and 1585 cm^{-1} associated with highly disordered

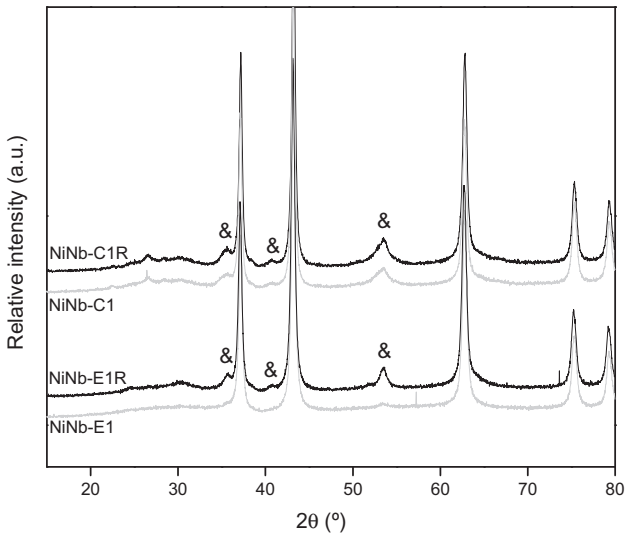

Fig. 12. XRD patterns for the mixed oxides before and after reaction. Ref.: (&) $NiNb_2O_6$.

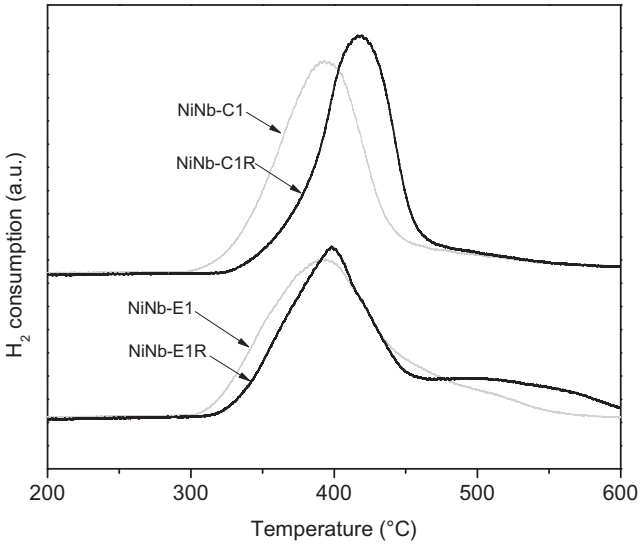

Fig. 13. TPR profiles of the mixed oxides before and after reaction.

Table 4
Surface Nb/Ni atomic ratio and morphological properties for mixed oxides before and after reaction (operating conditions: $O_2/C_2H_6/He = 5/5/90$, $F = 20\ cm^3/min$, $W/F = 0.54\ g\ s/cm^3$, $T = 400\ °C$).

Catalyst	Surface Nb/Ni atomic ratio*	S_{BET} (m^2/g)	Pore volume (cm^3/g)
NiNb-E1	0.10/0.90	81	0.182
NiNb-E1R	0.10/0.90	44	0.128
NiNb-C1	0.12/0.88	25	0.049
NiNb-C1R	0.13/0.87	20	0.047

* Determined by XPS.

graphitic carbon species [36,37] and derived from undesired reactions of hydrocarbon species on the catalyst surface.

Both spent catalysts showed a color change, from black for the fresh samples to green powders after reaction, which indicates the presence of stoichiometric NiO.

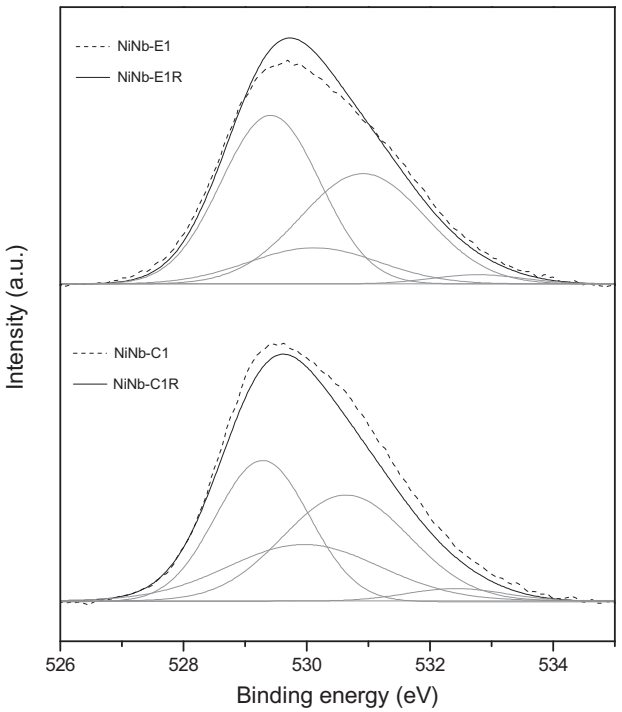

Fig. 14. X-ray photoelectron spectra of the O 1s region of fresh and spent catalysts.

In summary, in the case of the catalyst prepared by EM, no change in activity or selectivity was observed after 240 h of reaction. Although, there was an important decrease in specific surface area, that could be associated with the presence of carbon (Raman, see Fig. 15). The formation of the $NiNb_2O_6$ phase was also observed, without changes in the surface composition. On the other hand, in the case of the mixed oxide prepared by CS, a slight decrease in yield (3%) was observed, with no changes in the surface area or composition, and notably without the formation of carbon.

These observations highlight an important reduction in surface area for the NiNb-E1R catalyst that does not correlate with the observed constancy in activity.

As referenced, Savova et al. [11] studied the stability of the mixed oxide under similar operating conditions (380 °C for 290 h). They observed a mild deactivation of the mixed oxide with time on stream, and also a decrease in the specific surface area of the catalyst. However, they concluded that both events were not coupled, and deactivation may be ascribed to the formation of the crystalline phase $NiNb_2O_6$.

Skoufa et al. [38] investigated the catalyst deactivation at 400 °C for 100 h, and reported the same behavior: slight catalyst deactivation accompanied by a ~40% reduction in surface area. Unlike previous reports [11], the formation of $NiNb_2O_6$ was not observed.

Experiences not shown in the presented manuscript revealed mass transfer limitations when operating at 400 °C in conditions of Fig. 10 (feed flowrate = 20 cm^3/min) and kinetic control in conditions of Fig. 8 (feed flowrate = 40 cm^3/min).

For the former case, no change in activity or selectivity was observed for the catalyst prepared by EM after 240 h of reaction, but these results shown an apparent activity since the experience was not performed under pure kinetic control. Under these conditions, observed reaction rates are independent of the concentration of active sites. In contrast, Fig. 8 shows that the activity of NiNb-E1 was variable during the stability test. In the latter condition, the slight activity loss observed for NiNb-E1 catalysts could possibly be associated with the carbon formation during reaction. Regarding the formation of the crystalline phase $NiNb_2O_6$ during reaction and its relationship with catalyst deactivation, the results were not conclusive. In fact, the formation of the phase $NiNb_2O_6$ was observed for NiNb-E1R, but no changes were observed for NiNb-C1R. However, the NiNb-C1R sample also presents a decrease in conversion.

4. Conclusions

The catalyst prepared by combustion synthesis, a technique that is simpler than the conventional evaporation method, exhibited a good activity and stability compared with those observed for the catalyst synthesized by the evaporation method, even for long-term tests. Regarding the effect of the metal precursor, nickel nitrate and ammonium niobate oxalate generated the better catalyst in both synthesis routes.

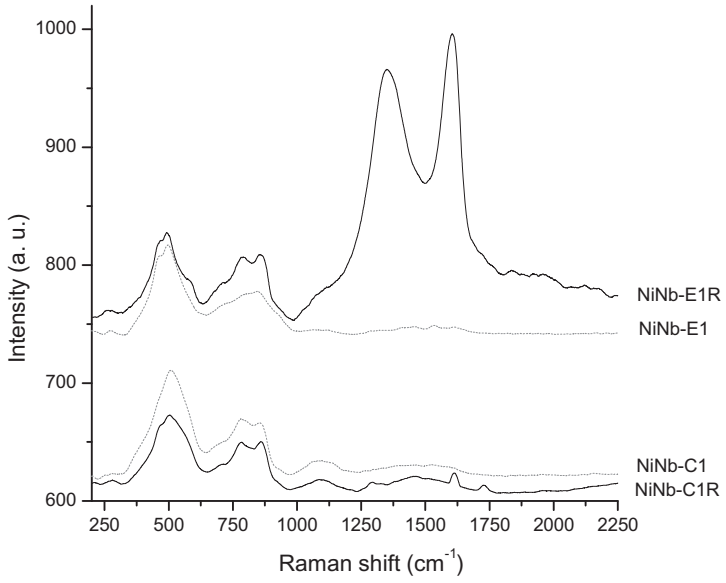

Fig. 15. Raman spectra of the mixed oxides before and after reaction.

The catalysts synthesized in the present work showed an almost constant ethylene yields for 120 h in stream at 400 °C at W/F = 0.06 g s/cm^3 (8% and 15% for combustion and evaporation synthesis, respectively) with a slight decrease over time on stream (13% and 11%).

Surface activity for ethane consumption and ethylene formation were higher than those observed for the sample prepared by the evaporation method and with the same precursor drug. This catalytic performance could be associated to a better utilization of the active sites due to a higher accessibility of the reagents to the catalyst surface, considering the observed similarities in the chemical aspects of the surface but observed differences in the morphological properties.

The experimental results suggest that further improvements in the NiNb-C1 mixed oxide, especially increasing surface area, can be expected upon optimization of the preparation method.

Acknowledgements

The authors thank ANPCyT (National Agency of Scientific and Technological Promotion, Argentina) and CONICET (National Council for Scientific and Technological Research, Argentina) for the financial support. Purchase of the SPECS multitechnique analysis instrument (PME8-2003) by ANPCyT is also acknowledged.

References

[1] T. Ren, M. Patel, K. Blok, Energy 31 (2006) 425–451.
[2] M. Neelis, M. Patel, K. Blok, W. Haije, P. Bach, Energy 32 (2007) 1104–1123.
[3] J.P. Bortolozzi, T. Weiss, L.B. Gutierrez, M.A. Ulla, Chem. Eng. J. 246 (2014) 343.
[4] L. Basini, S. Cimino, A. Guarinoni, G. Russo, V. Arca, Chem. Eng. J. 207–208 (2012) 473–480.
[5] G. Che-Galicia, R. Quintana-Solórzano, R.S. Ruiz-Martínez, J.S. Valente, C.O. Castillo-Araiza, Chem. Eng. J. 252 (2014) 75–88.
[6] G. Karamullaoglu, S. Onen, T. Dogu, Chem. Eng. Process. 41 (2002) 337–347.
[7] J.M. López Nieto, P. Botella, P. Concepción, A. Dejoz, M.I. Vázquez, Catal. Today 91–92 (2004) 241–245.
[8] B. Solsona, J.M. López Nieto, P. Concepción, A. Dejoz, F. Ivars, M.I. Vázquez, J. Catal. 280 (2011) 28–39.
[9] P. Botella, A. Dejoz, J.M. LópezNieto, P. Concepción, M.I. Vázquez, Appl. Catal A 298 (2006) 16–23.
[10] E. Heracleous, A.A. Lemonidou, J. Catal. 237 (2006) 162–174.
[11] B. Savova, S. Loridant, D. Filkova, J.M.M. Millet, Appl. Catal. A Gen. 390 (2010) 148–157.
[12] B. Solsona, P. Concepción, B. Demicol, S. Hernández, J.J. Delgado, J.J. Calvino, J.M. López Nieto, J. Catal. 295 (2012) 104–114.
[13] E. Heracleous, A.A. Lemonidou, J. Catal. 270 (2010) 67–75.
[14] H. Zhu, S. Ould-Chikh, D. Anjum, M. Sun, G. Biausque, J. Basset, V. Caps, J. Catal. 285 (2012) 292–303.
[15] E. Heracleous, A.A. Lemonidou, J. Catal. 237 (2006) 175–189.
[16] C.N.R. Rao, Chemical Approaches to the Synthesis of Inorganic Materials, Wiley Eastern Limited, 1993. 28–30.
[17] A.G. Merzhanov, J. Mater. Process. Technol. 56 (1996) 222–241.
[18] S. Biamino, C. Badini, J. Eur. Ceram. Soc. 24 (2004) 3021–3034.
[19] S. Pengpanich, V. Meeyoo, T. Rirksomboon, J. Schwank, J. Nat. Gas Chem. 16 (2007) 227–234.
[20] A.C. Faro, P. Grange, A.C.B. dos Santos, Phys. Chem. Chem. Phys. 4 (2002) 3997.
[21] M.A. Langell, C.L. Berrie, M.H. Nassir, K.W. Wulser, Surf. Sci. 320 (1994) 25.
[22] D. Stosic, S. Bennici, V. Rakic, A. Auroux, Catal. Today 192 (2012) 160–168.
[23] M. Francisco, R. Landers, Y. Gushikem, J. Solid State Chem. 177 (2004) 2432–2439.
[24] V.J. Ferreira, P. Tavares, J.L. Figueiredo, J.L. Faria, Catal. Commun. 42 (2013) 50–53.
[25] A. Carley, S. Rassias, M. Roberts, Surf. Sci. 135 (1983) 35.
[26] B.P. Payne, M.C. Biesinger, N.S. McIntyre, J. Electron Spectrosc. Relat. Phenom. 185 (2012) 159–166.
[27] M.W. Roberts, R.T.C. Smart, in: J. Chem. Soc. Faraday Trans. 80 (1984) 2957–2968.
[28] J.-M. Jehng, I.E. Wachs, Chem. Mater. 3 (1991) 100–107.
[29] M.P.F. Graça, A. Meireles, C. Nico, M.A. Valente, J. Alloys Comp. 553 (2013) 177–182.
[30] I. Nowak, M. Ziolek, Chem. Rev. 99 (1999) 3603–3624.
[31] M.O. Guerrero-Pérez, J.L.G. Fierro, M.A. Bañares, Phys. Chem. Chem. Phys. 5 (2003) 4032.
[32] S.S. Nkosi, B. Yalisi, D.E. Motaung, J. Keartland, E. Sideras-Haddad, A. Forbes, B.W. Mwakikung, Appl. Surf. Sci. 265 (2013) 860–864.
[33] S.I. Cordoba-Torresi, A. Hugot-Le Gaff, S. Joiret, J. Electrochem. Soc. 138 (1991) 1554–1559.
[34] B.M. Weckhuysen, Chem. Commun. 2 (2002) 97–110.
[35] Z. Skoufa, E. Heracleous, A.A. Lemonidou, Catal. Today 192 (2012) 169–176.
[36] P. Petersen, W. Krasser, Appl. Surf. Sci. 103 (1996) 91–100.
[37] E. Cao, M. Sankar, S. Firth, K. Fung Lam, D. Bethell, D.K. Knight, G. Hutchings, P. McMillan, A. Gavriilidis, in: Chem. Eng. J. 167 (2011) 734–743.
[38] Z. Skoufa, E. Heracleous, A.A. Lemonidou, Chem. Eng. Sci. 84 (2012) 48–56.